Lysine metabolism conveys kidney protection in hypertension

Markus Rinschen
Scripps Research Institute https://orcid.org/0000-0002-9252-1342
Oleg Palygin
Medical College of Wisconsin https://orcid.org/0000-0002-3680-5527
Daria Golosova
Medical College of Wisconsin https://orcid.org/0000-0002-9663-9639
Xavier Domingo-Almenara
The Scripps Research Institute https://orcid.org/0000-0002-0133-6863
Amelia Palermo
The Scripps Research Institute
Michael Schafroth
The Scripps Research Institute https://orcid.org/0000-0002-5864-6766
Carlos Guijas
The Scripps Research Institute
Megan Gliozzi
Division of Renal-Electrolyte
Jingchuan Xue
Scripps Research
Martin Höhne
University of Cologne https://orcid.org/0000-0001-8698-5389
Thomas Benzing
University Hospital, University of Cologne, Cologne, Germany https://orcid.org/0000-0003-0512-1066
Bernard Kok
Scripps Research
Enrique Saez
The Scripps Research Institute https://orcid.org/0000-0001-5718-5542
Markus Bleich
Kiel University https://orcid.org/0000-0002-1745-2295
Nina Himmerkus
Christian-Albrechts-University
Ora Weisz
University of Pittsburgh
Benjamin Cravatt

Scripps Research Institute https://orcid.org/0000-0001-5330-3492
Marcus Krüger
University of Cologne https://orcid.org/0000-0002-5846-6941
H. Paul Benton
The Scripps Research Institute https://orcid.org/0000-0002-4248-2269
Gary Siuzdak (siuzdak@scripps.edu)
Scripps Research Institute https://orcid.org/0000-0002-4749-0014
Alexander Staruschenko
Medical College of Winsconsin https://orcid.org/0000-0002-5190-8356

Article

Keywords: hypertension, kidney disease, lysine metabolism

Posted Date: November 30th, 2020

DOI: https://doi.org/10.21203/rs.3.rs-108965/v1

Version of Record: A version of this preprint was published at Nature Communications on July 14th, 2022. See the published version at https://doi.org/10.1038/s41467-022-31670-0.

Abstract

Hypertension and kidney disease, two related, common, and severe disease entities, have been repeatedly associated with genomic variants and metabolic alterations of lysine metabolism. Here, we developed a stable isotope labeling strategy compatible with untargeted metabolomics acquisition to investigate the physiology and molecular spectrum of lysine's metabolic fate in vivo. Mice received 13C6 labeled lysine through the diet over two months to track more than 100 lysine metabolites across various organs and body fluids. Lysine reacts rapidly with molecules of the central carbon metabolism, as opposed to slow or incorporation into proteins and metabolization into acylcarnitines. The kidney rapidly forms these lysine conjugates and lysine metabolism is decreased in early stages of hypertension. Lysine administration completely diminished the development of salt-sensitive hypertension and kidney injury in the Dahl salt-sensitive rat model. Administration of lysine leads to diuresis, acceleration of 13C6 lysine conjugate formation, and inhibition of albumin uptake, thereby protecting from nephron injury and metabolic stress. Lysine conjugates with malonyl-CoA to form a novel metabolite Ne-malonyl-lysine to inhibit fatty acid synthesis. Formation of Ne-malonyl-Lysine, and acetyl-Lysine during lysine treatment depletes malonyl-CoA and acetyl-CoA, respectively, a process that occurs at the expense of protein malonylation and acetylation. A significant fraction of lysine molecules was metabolized in the kidney and excreted as fructoselysine and saccharopine, via the urine, leading to an overall depletion of central carbon metabolites from the organism. A ketogenic diet also ameliorated hypertension, yet to a lower extent, and increased several lysine conjugates, including Ne-malonyl-lysine. In conclusion, isotope tracing of orally administered lysine illuminated lysine metabolism, and L-lysine protects the kidneys in metabolically defined subtypes of kidney disease.

Key Points

- The kidney is a key organ for lysine metabolism and lysine modification as revealed by untargeted *in vivo* isotope based metabolomics.
- Excess lysine is an effective treatment of a rat model of salt-sensitive hypertension that leads to the formation of kidney-protective metabolites and inhibition of proximal tubule albumin uptake.
- Lysine-dependent formation of Ne-malonyl-lysine, a novel discovered metabolite, depletes malonyl-CoA pools in the tissue, reduces protein malonylation, and correlates with decreased abundance of free fatty acids.
- Lysine excretion occurs as conjugates such as Ne-fructoselysine, and saccharopine in the hypertensive kidney, and results in a negative balance on central carbon and carbohydrate metabolism.
- Increased modified lysine molecules, including malonyl-lysine are also observed in kidney tissue of rats fed a ketogenic diet, a second antihypertensive and kidney-protective metabolic intervention.

Introduction

In the past decade, the role of amino acid metabolism has extended from a provider of protein building blocks to a decisive element in various physiological processes and diseases[1,2]. The amino acid lysine is an essential amino acid that is at the crossroads between proteins and metabolism and is of interest as both drug target and modifier of protein activity[3–5]. Lysine incorporated into proteins is heavily modified with an increasing number of molecules such as organic carboxylic acids[6–10]. Lysine from protein residues also gives rise to carnitines with a central role in beta oxidation. Multiple molecular lysine degradation and modification reactions are known. In this context, lysine's metabolism and its related bioactivity[11] has not been studied in a systematic fashion. Untargeted metabolomics offers the ability to identify altered and previously undescribed physiologically relevant molecules[11]. When applied together with isotope-labeling (using ^{13}C labeled molecules), kinetics of synthesis and degradation can be quantified, and novel metabolites can be discovered.

The kidney is a central hub of mammalian metabolism, but its metabolic importance is relatively understudied. With up to one out of ten persons suffering from kidney disease, kidney diseases pose a significant socioeconomic burden[12]. Hypertension, potentially caused by kidney disease, is also an epidemic, and both entities are strongly associated[13]. Multiple genome-wide association studies have highlighted the role of carnitine metabolism and lysine transport (via kidney-specific transporter SLC7A9)[14–16] in kidney disease. Metabolomic biomarker studies in the Framingham cohort, one of the most important cohort for prediction of cardiovascular outcomes, showed that high abundance of lysine in the urine is protective[17]. Three randomized controlled trials (RCTs) in humans performed untargeted metabolomics of serum and urine under dietary conditions beneficial for hypertension (so-called DASH diet, or sodium restriction)[18–20], and found association with high signals of lysine, or modified lysine, with protective interventions.

The aim of this paper was to establish an untargeted metabolomics workflow to interrogate ten body organs of a mouse that were fed with an isotope labeled diet $^{13}C_6$ lysine chow for up to two months, and to utilize this knowledge to intervene with hypertensive kidney disease. The analysis revealed that the kidney is strongly involved in handling lysine metabolites, with a specific bias towards conjugating free lysine to modifications at a faster speed. Notably, because of the identity of lysine conjugated molecules formed, and lysine's metabolic activity, strong metabolic alterations driven by excess lysine orchestrate a kidney-protective effect in hypertension.

Results

Adult male mice were fed with normal diet and were switched to food containing exclusively $^{13}C_6$ lysine for 0 (control), 1, 2, and 8 weeks (Fig. 1A). Unlabeled mice served as a control. A significant shift in global metabolomics features occurred depending on the duration of the diet (Fig. S1A). The analysis consisted of two approaches: 1) a mass-difference approach that looks for coeluting peaks (modified from previous protocols[21]), and 2) a correlation-based approach that extracts the mass trace of provided compounds and uses correlations to call out isotopologues. The analysis revealed 66 metabolites

(approach 1) as well as 133 metabolites (approach 2) that were validated using standards and fragmentation MS2 spectra (Fig. 1B). A significant overlap of validated metabolites was found by both methods. Overall correlation of extracted and verified metabolites was higher than other, non-verified metabolites (Fig. S1 B, C). Analysis of isotopologue patterns revealed that virtually all these metabolites were labeled with $^{13}C_6$ or $^{13}C_4$ atoms, meaning their entire carbon backbone was incorporated (Fig. 1C). Rates of $^{13}C_4$ incorporations were significantly slower incorporated as compared to C6 units (Fig. S1 D). We then separated the labeled peaks into different classes of lysine metabolites that included lysine, lysine degradation products such as saccaropine, pipecolic acid and aminoadipic acid, modified lysines such as N- and E-acetylation, methylation, hydroxylation and many others, carnitine synthesis products such as trimethyllysine, lysine-containing peptides and several acetylcarnitines. Detected lysine metabolites as well as chemical information are listed in TABLE S1 and S2. In general, we found using both methods that lysine had the highest incorporation slope among the metabolites, followed by lysine degradation and modification, and by peptides. In general, incorporation of lysine into acylcarnitines was slower than other metabolic processes (Fig. S1D). We calculated the slope of different classes of metabolites using a linear model during the first two weeks. Notably, we did not observe any labeling in $^{13}C_2$ units (such as glycine), and targeted analysis of the TCA cycle metabolites revealed no significant incorporation of TCA metabolites in the TCA cycle in any tissue (summary in Fig. S2). Analysis of the diet using untargeted metabolomics revealed that the food had no detectable amount of carnitines, and other lysine metabolites in the diet (Fig. S1). Comparison of different organs was performed next, and slopes of incorporation were summed and plotted. Organ-specific incorporation rates (plotted as slope of difference of leading C_{13}/C_{12} isotope) of lysine metabolite classes were distributed to the different organs (Fig. 1D). In the thymus, we observed several lysine incorporated peptides that were represented in this organ. The analysis revealed that the kidney cortex was one of the fastest incorporating organs, especially for modified lysines, peptides, and acylcarnitines. (Fig. 1D). Kidney and liver showed both the highest incorporation rates, but the kidney had a higher incorporation rate for Ne-Fructosyl-lysine (Fig. 1E).

We then sought to integrate metabolome and proteome in an independent experiment. Kidney cortex tissue from mice fed with $^{13}C_6$ lysine for 1, 2, and 3 weeks were analyzed. Since lysine also gets incorporated into proteins, we determined both the metabolome and the proteome from these samples. We plotted the logarithmic ratios of the maximum isotopologue (peptides labeled with a mass shift of 6 Da) over control (Fig. 1F). The isotopologue ratio for lysine was higher than any other molecule, followed by metabolites from the lysine degradation pathway, and modified lysines. Proteins were incorporated significantly slower as compared to lysine metabolite, and histone and DNA-binding proteins had the lowest incorporation rate among proteins (Fig. 1F). Metabolites ratio of labeled over unlabeled molecules had a wider distribution compared to proteins (Fig. 1G). To further investigate if protein incorporation is different in the medulla, we micro-dissected the kidneys in four macroscopic areas: outer stripe cortex, outer stripe medulla, inner stripe outer medulla, and inner medulla (FIG. S3A). We found that the lysine protein incorporation was slower in the medullary areas, consistent with the known metabolic role of the proximal tubule (FIG S3B). Taken together, these data suggests that the cortex, and specifically

the proximal tubules that comprise more than 80% of the cortex, is likely to be the major hub within the kidney for lysine metabolism.

We had earlier reported a deficit of lysine metabolites in the kidney cortex in a hypertensive kidney disease model[22]. Based on these findings, and on a potential beneficial role of lysine in the Framingham cohort[17] and 3 randomized controlled dietary intervention trials[18–20], we hypothesized that administration of lysine can be helpful in a model of hypertensive kidney disease. We subjected hypertensive rats to high abundance of lysine in the drinking water (Fig. 2A). Dahl Salt-Sensitive (D/SS) rats are a physiological relevant model of hypertension and hypertensive kidney disease that generates high blood pressure when fed a high salt diet. We monitored real-time blood pressure using telemetry over the entire time course of the disease (Fig. 2B). Both male and female rats on different salt diet regimens receiving lysine supplementation were largely protected with attenuated development of hypertension (Fig. 2B, Fig. S4A). Albuminuria, a readout of hypertensive kidney damage, was decreased in various regiments (Fig. 2C, Fig. S4B). The excretion of potassium, as well as excretion of urinary metabolites/electrolytes did not change between lysine treated and non-treated rats, suggesting that hypertension-inducing salt diet was not taken up to a different extent (FIG. S4C). Automated histology analysis using convoluted neural nets[23] revealed a significant improvement in ultrastructure of glomeruli by lysine (based on quantification of more than 3500 glomeruli/group) (FIG. S4D).

To understand lysine handling in high and low lysine conditions, we performed *in vivo* isotope labeling of $^{13}C_6$ lysine in lysine treated and non-treated hypertensive rats. We injected lysine-treated and lysine-untreated rats with a defined bolus of $^{13}C_6$ lysine (Fig. 2D) and analyzed urine (collected 24 hrs), serum and kidney tissue for incorporated lysine metabolites. More $^{13}C_6$ labeled lysine was detected in urine of ad libitum lysine-treated rats (Fig. 2E). We also found an increased abundance of $^{13}C_6$ labeled saccharopine, and fructoselysine in urine (normalized by creatinine), while $^{13}C_6$ incorporation in the kidney was reduced (Fig. 2E). Consistent with an increased lysine clearance, physiological studies measuring 24 hrs urine revealed that lysine induced diuresis (Fig. 2F), a finding observed after only 1 day of lysine treatment (Fig. S4E).

Hypertension results in proteinuria, and proteinuria itself is further detrimental for kidney function when urinary proteins, especially albumin, is taken up by the proximal tubule, the predominant cell type within the kidney cortex [24]. Therefore, we hypothesized that albumin uptake in the proximal tubule was blocked or altered by lysine, supported by previous *in vitro* and *in vivo* findings[25] in a physiological context. Consistent with this hypothesis, lysine administration itself in D/SS rats on a normal salt diet induced an increase in urinary albumin (Fig. 3A). Cell culture studies using Opossum Kidney (OK) proximal tubule cells revealed that even moderate addition of lysine decreased uptake of fluorophore labeled albumin (Fig. 3B), a key function of proximal tubules. Basolaterally-applied lysine (2 hr, 50 mM) inhibited uptake of albumin and the fluid-phase marker dextran (not shown), even when the cells were assayed 2 h after lysine washout (Fig. S5A). This is remarkable, because the receptor LRP2 responsible for albumin uptake is localized apically[26]. In addition, we observed that overnight incubation with lower doses of lysine

resulted in a profound and dose-dependent decrease in albumin uptake (half max inhibition at ~ 3.5 mM lysine) (Fig. S5B). Next, we examined hypertensive kidneys after dietary high-salt exposure *in vivo* using dual photon microscopy and fluorescently labeled albumin (Fig. 3C). Proximal tubules took up albumin and accumulate excessive albumin in luminal protein casts (arrows), suggesting that an overloading of the albumin uptake machinery occurs in hypertension. Consistently, lysine reduced albumin casts in kidneys as observed in Masson's trichrome staining (Fig. 3D). In immunohistochemistry staining, LRP2 (megalin) abundance, the chief lysine uptake mechanism protein inhibited by lysine, was decreased in dilated non-functional proximal tubules damaged by albumin[25]. This effect was completely diminished by lysine administration (Fig. 3D). Expression of kidney injury molecule-1 (KIM-1), a marker of proximal tubule injury, was strongly decreased with lysine as well, suggesting protection from tubule damage by lysine (Fig. 3D).

Combined, *in vivo* and *in vitro* observations argue for an effect of lysine beyond simple competitive inhibition of albumin binding to the apically-localized megalin and cubilin receptors[26]. To further investigate the mechanism, we examined the cortex metabolome (Fig. 3E). Kidneys from healthy rats (on a low-salt diet) did not change lysine or kidney metabolism at all when challenged with a high lysine intervention ($q < 0.05$). However, with increased disease severity, there were more alterations in lysine metabolites, and in general metabolism. Lysine was increased in hypertension, as also supported by HPLC analysis (Fig. S5C). We found that especially metabolites that had a faster incorporation in the initial experiment (such as Ne-Acetyllysine, saccharopine, and Fructose-lysine), were increased through the lysine challenge, suggesting these metabolites serve as an "overflow" (Fig. 3E). Further analysis of the dataset suggested that free fatty acids (FFA) were altered by lysine supplementation (Fig. 3F), with a strong decrease in the most severe damage condition. The entire class of FFA (n = 22 quantified molecules) showed a strong and distinct downregulation, with linoleic acid being decreased by lysine treatment in every single condition. Further examination of the dataset revealed a reduction of glucose and other sugar metabolites. NAD^+, a kidney protective molecule associated with decreased oxidative stress, was increased with lysine treatment in the severe conditions (Fig. 3G).

We hypothesized that lysine's tendency to form conjugates was responsible for reduction in the FFAs. We examined the isotope labeling dataset for lysine conjugates that could be responsible for a decrease in fatty acid building blocks. Careful examination of the unknown peaks in the untargeted metabolomics isotope study revealed the presence of a mass consistent with Nε-malonyl-lysine in the kidney and liver (Nε-malonyl-lysine, m/z [H+] of 233.11 and m/z as a Na adduct of 255.10) (Fig. 4A). This molecule is a previously undescribed novel metabolite without a Pubchem entry. Synthesis of a standard, together with retention time comparison (Fig. S6A,B, Supplemental material and methods) confirmed the identity of the compound as Nε-malonyl-lysine (Fig. 4B), and targeted analysis using MRM showed labeling only the $^{13}C_6$ lysine containing kidney tissue (Fig. S6F). In order to understand if malonyl-lysine would form enzymatically or chemically, we analyzed whether it would form in alkaline conditions from the educts malonyl-CoA and lysine (1:10 w/w) ratio. We observed that < 1% of lysine molecules were malonylated (Fig. 4B). We found that Nε-malonyl-lysine was significantly increased in the hypertensive kidneys with

lysine (Fig. 4C), suggesting that supraphysiological lysine supplementation could deplete the abundance of malonyl-CoA, a substrate of fatty acid synthesis and an inhibitor of fatty acids. Consistently, we observed significant decrease of malonyl-CoA (Fig. 4D). In addition, Nε-acetyl-Lysine was increased by lysine treatment (Fig. 4E). Acetyl-CoA was decreased in at least one lysine treatment condition and trended to be reduced in the other two conditions (Fig. 4F). While the free acetyl-lysine and Nε-malonyl-lysine were increased, protein modification through these metabolites decreased as evidenced by immunoblotting (Fig. 4G). These findings suggest that the chemical modification of lysine occurs in the kidney to deplete important anabolic molecules Acetyl-CoA and malonyl-CoA.

We then analyzed the metabolic changes in a more integrative fashion, evaluating both matched tissue, urine, and serum from the same animals, and calculating correlation coefficients between individual metabolites in different compartments. Integrative analysis of correlations between tissue and urine metabolites revealed that urinary lysine was strongly associated with tissue lysine and tissue lysine degradation products (Fig. 5A). High lysine in the urine was also negatively correlated with proteinuria (Fig. 5B). Interestingly, urinary lysine was also negatively correlated with the abundance of sugar molecules, such as glucose, glucose-6-phosphate, and sucrose. In fact, targeted analysis revealed a decrease in glucose abundance in the cortex. Together with an increase of Nε-fructoselysine in the urine this suggests a net glucosuric effect. Interestingly, this effect was stronger in severely damaged cortices. Lysine treatment also induced loss of other amino acids under these conditions, consistent with previous reports (Fig. 5C). The strongest excretion of lysine was as a sugar conjugate (fructoselysine), acetyl-CoA (acetyl-lysine), and α-ketoglutarate (saccharopine) in the damaged conditions (Fig. 5C). Analysis of lysine stoichiometry (mol/per ug creatinine) revealed that most of the excreted lysine was in the unmetabolized form. However, the excretion of lysine in the form of saccharopine, fructoselysine was more significant when kidneys were protected by lysine (Fig. 5D). Using targeted metabolomics, we confirmed the decrease of glucose and glucose-6-P in the tissue, but there was no altered abundance of these metabolites in the urine. The tissue abundance of the final metabolites of the TCA cycle, fumarate, and malate, were significantly depleted by lysine (Fig. 5E), although their urinary excretion was not altered (not shown). Metabolomic analysis of serum revealed that in hypertension, there were no major changes in fructoselysine, saccharopine, acetyl-lysine, and others (Fig. S7), as opposed to control rats. Taken together, these results suggest that excessive lysine reacts with active metabolites of the central carbon mechanism to excrete them, suggesting metabolic alterations may play a role in the beneficial effects of lysine in this model.

Lysine administration caused a net loss of glucose by forming Nε-fructoselysine, and a net loss of metabolites of anabolic processes, such as acetyl-CoA, malonyl-CoA and TCA cycle intermediates. This situation could be consistent with a local catabolic state, like ketosis. Therefore, we checked whether a ketogenic diet was able to yield a protective effect in the same model, and alter lysine metabolism (Fig. 6A). In fact, the rats were protected from hypertension (Fig. 6B, Fig. S8), but still developed proteinuria. Metabolic analysis of the tubules showed that lysine, acetyl-lysine, saccharopine, adipic acid and galactosyl-hydroxylysine were significantly increased along with precursors of ketone bodies, while central sugar metabolites were expectedly decreased (Fig. 6C). Consistent with the behavior of these

lysine conjugates, Nε−malonyl-lysine metabolite was also increased, suggesting that reduced availability of hexose to bind lysine was causing shifts to other lysine conjugates (Fig. 6D). The data support the role of metabolic interventions with lysine in kidney disease (Fig. 6E), and demonstrate lysine-dependent processes controlling physiology and metabolism of the kidney.

Discussion

Alterations in lysine metabolism are commonly observed in patients obtaining diets protective from hypertension[18–20], and lysine transport also associates with kidney function across multiple GWAS and mGWAS studies. High abundance of lysine in the urine (associated with variants in the tubular lysine uptake transporter SLC7A9) associated with a good prognosis[17], and these findings were replicated in another CKD cohort[14]. The important role of lysine for kidney disease is also supported by animal studies suggesting that lysine supplementation does not alter lysine in the serum, but has effects on secondary disease entities in the bone[27]. Together, these data demonstrate that differential amino acid metabolism can be a potential target for diseases at the interface of hypertension and kidney disease.

Here, we develop a technology to utilize untargeted metabolomics workflows in order to quantify lysine fate across tissues. Isotope tracing methods usually use targeted metabolomics in order to develop hypothesis-driven views or models of metabolism. To catalogue as many molecules as possible, we performed global untargeted metabolomics analyses to identify labeled metabolites[28,29]. This workflow compares lysine metabolites in extension of previous studies that focused on protein incorporation[30–32]. The approach used here comes with some limitations of untargeted metabolomics, but also has several key advantages. First, one can catalogue the entity of metabolites of a distinct molecule at a broader depth as targeted approaches. Second, it allows to discover new and biologically important molecules from untargeted isotope labeled metabolomics data. The use of labeling at high percentages (over 95% of labeled lysine molecules were labeled) enables identification of significantly incorporated metabolites *in vivo*. The feeding through the diet (as opposed to parenteral administration) enables analysis of microbiome-derived metabolites. The combination of untargeted isotope-based metabolomics and proteomics suggested that lysine is replaced faster with $^{13}C_6$ units before it is incorporated into the proteins and carnitines. This suggests a major network of lysine modification (“epimetabolome”) independent of the incorporation of metabolites into proteins, and that the main pool of free modified lysines derive from direct chemical and enzymatic reactions[5], and not from protein modifications such as histones.

The observation of molecular Nε−malonyl-lysine, a previously unidentified metabolite, was only possible through the *in vivo* isotope labeling approach. We suggest that the malonyl-Lysine metabolite is formed – enzymatically or non-enzymatically – via the reaction with malonyl-CoA, the elongator of fatty acid synthesis, and an important anabolic metabolite. In fact, we observed lysine-dependent decrease in free fatty acids in the kidney cortex, but not in serum and urine, suggesting a renal specific effect. This also suggests that concentrations of lysine in the kidney are predisposing for the formation of the metabolite.

The alteration of FFA synthesis by NE-malonyl-lysine might also be of importance to general mechanisms of fibrosis development[33].

We used lysine administration to investigate kidney-specific lysine handling in hypertension. Lysine strongly decreased blood pressure, proteinuria, tissue damage and increased NAD+, a kidney-protective metabolite[34–36], while at the same time increasing diuresis. The proteinuria is particular relevant because lysine itself blocks albumin uptake, and induces a mild proteinuria in normal conditions (Fig. 3). Several previous studies suggested the presence of detrimental lysine modifications in hypertension[37,38]. Our study suggests that administration of lysine leads to conjugation of lysine to central carbon molecules, while it prevents these molecules to modify proteins. Mechanistically, these processes lead to diuresis that flushes out the protein plaques formed in the tubule system. Metabolically, this is beneficial because the lysine is excreted in modified forms: one prominent and fast lysine overflow system is the lysine-conjugation to central carbon metabolites. Acetyl-CoA, and glucose, form acetyl-lysine and fructoselysine (Amadori reaction), respectively. Formation of saccharopine consumes NADH and alpha-ketoglutarate and generates NAD and Glutamate. Together, this depletes metabolites of the central carbon metabolism from the kidney. The depletion of central carbon metabolites from the kidney is reminiscent of the effect of SGLT2 inhibitors, a recent breakthrough intervention to delay the outcome of cardiovascular kidney disease[39,40]. In fact, the quantitatively most important excretion mode of lysine was Fructosyl-lysine. Similar to the lysine challenge, ketosis of the entire body led to a depletion of sugars in the kidney cortex and increased Nε–malonyl-lysine, as well as saccharopine, presumably because more lysine is freely available. Notably, this metabolic intervention could also ameliorate hypertension, but kidney damage was altered to a lesser degree. Ketogenic diet has been a successful intervention to kidney diseases such as polycystic kidney disease[41] commonly associated with high blood pressure.

In conclusion, the analysis of labeled metabolites demonstrated the kidney-specific role of lysine metabolites, and its physiologic activity. Kidney protective effects in hypertension occur via lysine's unique physiology in the tubules and via its chemically modified entities that provide a sink for important sugar metabolites of the central carbon metabolism and fatty acid metabolism. Thus, lysine's metabolic activity alters the epimetabolome for kidney protection.

Methods

$^{13}C_6$ Lysine isotope labeling study.

Male Bl6/N mice (12 weeks old) were fed a custom diet (Silantes) containing more than 99% $^{13}C_6$ lysine. The protocol for labeling was described previously[30]. After 1, 2, and 8 weeks (protocol 1) or 1, 2, and 3 weeks (protocol 2), mice were sacrificed and perfused with ice-cold PBS. All denominated organs were snap-frozen from the same mouse and stored at -80 °C degrees. Blood was separated in erythrocyte and plasma by centrifugation.

Metabolomics sample preparation.

Frozen organs were kept on dry ice and 10 mg tissue was weighed. Then, 800 ul ice-cold extraction solution containing Acetonitril : Methanol : Water 2:2:1 was added. Samples were subjected to tissue homogenization using a multiplex-bead-beater (Storm) for 30 sec (liver), 1 min (lung), or 45 sec (all other tissues). The supernatant was transferred to a prechilled Eppendorf tube. Then, beads were washed with 200 ul of the extraction solution, and the wash solution was added to the remaining homogenate. The homogenate was incubated at -20 °C degrees for 2 hrs. Then, tissue was spun down at 4 °C degrees for 20 min, and the supernatant was transferred to another vial. The supernatant containing the extract was transferred into a speed vac and dried down. The next morning, the dried-down extract was once resuspended in 100 ul (per 10 mg tissue) of acetonitrile-water 1:1, and the solution was centrifuged at 4 °C degrees. Then, the solution was transferred to autosampler vials and stored at -80 °C until further use.

Untargeted metabolomics analysis and mass spectrometry.

LC-MS/MS analysis for metabolomics was performed as previously described[22]. Data was annotated with in-source fragments and adducts. Quality controls were run every 5 samples. The mass spectrometer was initially calibrated using NaFormate peaks and in addition post-run. For untargeted metabolomic analysis, we used a UHPLC-MS approach. For fractionation, we used hydrophilic interaction liquid chromatography (HILIC) fractionation and reversed-phase (RP) chromatography as previously described[22]. We used a quadrupole time-of-flight instrument (Impact II, Bruker, Bremen, Germany) coupled to a ultrahigh-performance liquid chromatography (UHPLC) device (Bruker Elute, Bruker, Billerica, MA), or to an Agilent Infinity 1290 UHPLC device (Agilent, USA). The MS was calibrated using sodium formate (post-run mass calibration). Data were acquired over an m/z range of 50 to 1000 Da in positive ion mode and negative ion mode (HILIC only). Electrospray source conditions were set as follows: end plate offset, 500 V; dry gas temperature, 200 °C; drying gas, 6 liters/min; nebulizer, 1.6 bar; and capillary voltage, 3500 V.

To increase metabolome coverage and minimize ion suppression, we used a dual fractionation strategy. For RP separation, an ACQUITY BEH C18 column (1.0 × 100 mm, 1.7-µm particle size; Waters Corporation, Milford, MA) was used, and for HILIC fractionation, a ACQUITY BEH amide (1.0 × 100 mm, 1.7-µm particle size; Waters Corporation, Milford, MA) column was used. Flow was 150 µl/min, and a binary buffer system consisting of buffer A (0.1% FA) and buffer B (0.1% FA in acetonitrile) was used. The gradient for RP was: 99% A for 1 min, 1% A over 9 min, 35% A over 13 min, 60% A over 3 min, and held at 60% A for an additional 1 min. The gradient for HILIC consisted of 1% A for 1 min, 35% A over 13 min, 60% A over 3 min, and held at 60% A for an additional 1 min. The injection volume was always 2 µl. For molecule identification purposes, putative molecules of interest were fragmented using three different collision energies (10, 20 eV) or ramp collision energies (20 to 50 eV).

Untargeted metabolomics data analysis.

Bruker Raw files (*.d) were transformed into mzml files using the compassxport_converter.py script (Bruker). Then, data files were uploaded to XCMS online, and differential peaks were extracted in positive and negative ion mode[42]. Feature Detection was performed with the centwave method with the following options: ppm = 10, minimum peak width = 5, maximum peak width = 20, mzdiff = 0.01, Signal/Noise = 6, Integration method = 1, prefilter peaks = 3, prefilter intensity = 100, noise filter = 100. For Retention time correction, we used obiwarp method with profStep = 1. Alignment was perfomed with bw 05, minfrac = 0.5, mzwid = 0.015. mminsamp = 1, and max = 100. Statistical test was performed using an unpaired parametric t-test (Welsh), with post-hoc analysis = TRUE,. Statistical filtering was performed for priorization of features of interest, including a fold change of at least 1.5, and a *p*-value lower than 0.05, and a corrected *p* value (q-value) lower than 0.05. The analysis included PCA and multivariate analyses. Metabolites were identified based on 1) unique mass, 2) MS^2 spectra comparison to authentic standard 3) coelution with authentic standard, and 4) isotopic pattern. The following adducts were routinely considered : Na, H, for positive mode, and Cl, formate for negative mode. Intensity data were plotted using instantclue[32], ggplot2, or circosplot.R package.

Kidney dissection.

Kidney cortices were isolated under manual control (protocol 1, Fig. 1). Kidneys were manually dissected using a stereomicroscope. Based on anatomical criterions, the kidneys were dissected into cortex, inner stripe outer medulla, outer stripe outer medulla and inner medulla (protocol 2, Suppl. Figure 3). The samples were snap-frozen and stored at -80 °C or dry ice.

Proteomics sample preparation.

Kidney samples of $^{13}C_6$ labeled kidneys were subjected to proteomics analysis using a tryptic in solution digestion protocol followed by nLC-MS/MS analysis. In brief, kidney pieces were minced and homogenized using a glass homogenizer in 8M urea containing 10 mM Ammoniumbicarbonate as well as protease and phosphatase inhibitor cocktail (Thermo). The homogenate was spun down at 6 °C for 20 min, and the supernatant was kept for further analysis. A small aliquot was subjected to protein measurement using BCA assay (Thermo). The proteins were reduced and alkylated using 5 mM DTT (30 min) and 10 mM IAA (1 hr) in the dark. Then, urea concentration was diluted to < 2M and LysC (1:100 w/w) ratio was added, and the mixture was digested for 16 hrs at 37 °C. The next day, the reaction was terminated by addition of 2% formic acid. Peptides were desalted using in-house made stage-tips and analyzed by nLC-MS/MS.

Proteomics analysis.

The peptides were separated by reverse-phase nanoflow-LC-MS/MS analysis and sprayed into a quadrupole-orbitrap tandem mass spectrometer (qExactive plus, thermo scientific) as previously described[43]. Raw Proteomics data were parsed with MaxQuant v 1.5.3.3.[44], using a Uniprot RefSeq reference proteome database from Jan 2017, with using LysC (cuts after each Lysine) as a protease.

Multiplexicity of the analysis was 2, with 13C6 labels in proteins as a modification in the second channel. The analysis has been previously described[45]. The non-normalized ratios (Heavy/13C6 over Light12C6) were used for further analysis using Perseus[46] software suite and filtering for ratios in all experiments, as well as for annotation with GO terms.

Dahl salt sensitive (D/SS) rats.

The strain of re-derived Rapp Dahl SS rats used in studies (SS/JrHsdMcwi, **RRID:RGD_1579902**) has been inbred for more than 50 generations at Medical College of Wisconsin. Male and female animals at the age of 8 weeks were used for experiments. Rats were maintained on AIN-76A custom diet, either low salt (LS; 0.4% NaCl, # 113755, Dyets Inc.) or high salt (HS; 4% or 8% NaCl, # 113756 or # 100078, respectively, Dyets Inc.). Water and food were provided *ad libitum*.

Dahl SS (D/SS) rat is a widely used model of salt-induced hypertension and CKD. Since the derivation of the D/SS rat in 1962, there have been numerous phenotyping studies demonstrating the importance of the kidney in the regulation of blood pressure. Cowley et al. showed that upon consuming a high salt diet, the D/SS rat rapidly becomes hypertensive and exhibits severe renal damage, yet GFR is not changed until 10 days after consuming a high salt diet[47].

Lysine treatment study.

Experimental animals received either vehicle (water) or L-Lysine (17 mg/ml) via drinking water (n = 6 per group). Blood pressure was measured by telemetry. D/SS rats were anesthetized with 2–3% (vol/vol) isoflurane and a blood pressure transmitter (PA-C40; DSI) was surgically implanted subcutaneously, with the catheter tip secured in the abdominal aorta via the femoral artery. After a 3-day recovery period, blood pressure was measured with a DSI system (“telemetry”) in conscious, freely moving SS rats under HS diet protocol, similar to those described previously[48–50].

For urine collection, rats were placed in metabolic cages (no. 40615, Laboratory Products) for a 24 hrs urine collection. These urine samples were used to determine electrolytes, microalbumin, and creatinine. Whole blood and urine electrolytes and creatinine were measured with a blood gas and electrolyte analyzer (ABL system 800 Flex, Radiometer, Copenhagen, Denmark)[48]. Kidney function was determined by measuring albuminuria using a fluorescent assay (Albumin Blue 580 dye, Molecular Probes, Eugene, OR) read by a fluorescent plate reader (FL600, Bio-Tek, Winooski, VT).

Ketogenic diet study.

Male D/SS rats (n = 7 per group) were fed either control high salt diet (4% NaCl, # 113756, Dyets Inc.) or high salt ketogenic diet (Keto Diet 4% NaCl, TD.190564, Teklad Custom Diet) for 28 days. Food composition is depicted in supplementary Fig. 8A. Water and food were provided *ad libitum*. Blood pressure acquisition, urine and whole blood analyzes were performed as descried above in lysine treatment study.

Pulsed $^{13}C_6$ Lysine labeling in the SS rat.

Male D/SS rats on HS protocol were administrated with $^{13}C_6$ L-Lysine-2HCl (#1860969, Thermo Scientific) at day 13 HS diet (8% NaCl; 24 hrs before sacrifice). Intraperitoneal injection of $^{13}C_6$ L-Lysine-2HCl (340 mM; 200 µl of PBS solution) was performed 24 hrs before sacrifice.

Albumin uptake cell culture studies.

Confocal microscopy was used to detect uptake of fluorescent albumin (AlexaFluor-647 albumin, 40 µg/ml) in confluent monolayers of OK proximal tubule epithelial cells[51] (visualized by fluorescent F-actin, 488 nm), grown on transwell filters under orbital shear stress as previously described and coincubated with lysine or glycine[52]. Cells were incubated for 1 hr in serum-free culture media containing fluorescent albumin), after pretreatment of 5–50 mM L-Lysine (or other amino acids) for 2 h, or after overnight treatment with 1–10 mM L-Lysine. Treatment was performed from the apical side unless otherwise indicated. Cell-associated albumin was quantified by spectrofluorimetry.

Intravital dual photon microscopy.

All surgical, imaging, rat fluorescent albumin, and image analysis procedures were performed as described previously[53,54]. Imaging was conducted using an Olympus FV1000 microscope adapted for an intravital two-photon microscopy with high-sensitivity gallium arsenide nondescanned 12-bit detectors. Animals were anesthetized with pentobarbital sodium (50 mg/ml). A jugular venous line was used to introduce fluorescent rat albumin (Texas Red labeled) and high-molecular weight dextran (150 kDa FITC-labeled, TdB Consultancy, Uppsala, Sweden).

Immunohistochemistry.

Rat kidneys were fixed in 10% formalin and processed for paraffin embedding as previously described[55]. Kidney sections were cut at 4 µm, dried, and deparaffinized for subsequent labeling by streptavidin-biotin immunohistochemistry. After deparaffinization, slides were treated with a citrate buffer (pH 6) for total of 35 min. Slides were blocked with a perioxidase block (Dako, Coppenhagen, Denmark), avidin block (Vector Laboratories, Burlingame, CA), biotin block (Vector Laboratories), and serum-free protein block (Dako). Tissue sections were incubated for 90 min in antibody to Kidney Injury Molecule-1 (Rat KIM-1Ab, 1:300, #AF3689, R&D Systems, Inc) or megalin (lipoprotein-related protein 2 (LRP2) Ab, 1:2500, from Dr. Franziska Theilig University of Kiel, Kiel, Germany). Secondary detection was performed with goat anti-goat or anti-rabbit biotinylated IgG (Biocare, Tempe, AZ) followed by streptavidin-horseradish peroxidase (Biocare) and visualized with diaminobenzidine (Dako). All slides were counterstained with Mayer's hematoxylin (Dako), dehydrated, and mounted with permanent mounting medium (Sakura, Torrance, CA).

Bioinformatic image analysis via convolutional neural net analysis.

Rat kidneys were cleared of blood, formalin fixed, paraffin embedded, sectioned, and mounted on slides as previously described[56]. Slides were stained with Masson's trichrome stain. The localization and scoring of glomeruli was performed by a novel and robust application of convolutional neural nets[23,57]. A cumulative distribution plot was generated (OriginPro 9.0) using glomerular injury scores based on a scale of 0–4 as previously described[58], and the probability for a corresponding score interval was calculated (more than 3,500 glomeruli per group). Cortex protein cast analysis was performed using a color deconvolution filter and Analyze Particles mode in the Fiji image application (ImageJ 1.51u, NIH).

Bioinformatic algorithms for mass-difference based isotope selection.

Labeled isotopologues were detected using an in-house isotracker script (see Data Availability and github submission) that operated as follows: first, we search for groups of features that, according to their m/z difference (< 10 ppm), could correspond to an isotopic envelope composed of a light isotope and heavy isotopes. Only features within 2 seconds of retention time difference were allowed to be grouped into a single isotopic envelope. Next, we compared the isotopic envelope between labeled and unlabeled samples. The envelopes presenting at least one heavy isotope with statistically significant higher abundance in labeled samples compared to unlabeled samples were retained for further analysis.

Correlation-based isotope selection approach.

Labeled isotopologues were detected using an in-house script (see Data Availability and github submission) that operated as follows: The custom R script is designed to identify isotopes from stable labeled isotope LC-MS data based on an input list of compounds and sum formulas and is available online including documentation via https://github.com/hpbenton/targeted_isotopes. It uses mzR and MSnBase from the bioconductor repository to open and manipulate the data. Once the raw data is opened each file is independently searched for a list of possible compound hits. These compounds are searched by creating a small bin of a user chosen ppm range around the mass. The vector of data undergoes a smoothing using a Savitzky Golay filter. Any compound that is above a given threshold (default 1000 counts) and is also above the chosen signal to noise is selected. Then, since the formula is known, any and all isotopes are searched within the same ppm range and at that retention time range. If the isotope peak also satisfies the above criteria the two vectors are correlated to help confirm a true positive isotope. Most isotopes are correlated above 0.9[59], Supplemental Fig. 1. The script used a list of 400 lysine metabolites derived from KEGG and METLIN as input.

Synthesis of Nε-malonyl-Lysine.

For a detailed description of Nε-malonyl-Lysine and Nα-malonyl-lysine isomers, please see the supplementary material and methods. Molecules were synthesized as described in the supplementary materal and methods and characterized by NMR and mass spectrometry. Volatiles were removed under reduced pressure and the crude product was purified by mass directed preparative reversed phase HPLC to give the formic acid salt which was directly used as an analytical standard and fragmented at 10, 20 and 20–50 eV in ESI in positive ion mode.

Malonyl-CoA and lysine in vitro reaction.

1 uM lysine and a 10 uM of malonyl-CoA was incubated together in 10 ul of PBS, pH = 8 at 37 degrees for 1 h. Both the isotope-labeled ($^{13}C_6$) and non-isotope-labeled ($^{12}C^6$) form of lysine were used, in order to exclude unspecific molecule products. Mixtures were analyzed on a QQQ as well as a QTOF machine. Specific transitions were used in order to detect both heavy and light forms of N-e-malonyl-lysine as well as lysine, and malonyl-CoA.

Malonyl-CoA assay.

Malonyl-CoA levels from tissue lysates were determined using a commercial rat ELISA assay (MyBiosource.com) according to the manufacturer's manual.

Targeted metabolomics.

Targeted metabolomic analysis was performed on a triple-quadrupole (QQQ) mass spectrometer (Agilent Triple Quadrupole 6490, San Diego, CA), and the LC part was coupled to a high-performance liquid chromatography (HPLC) system (1290 Infinity, Agilent Technologies) coupled to ion funnel. For glycolysis and TCA product metabolite, a ZIC-pHILIC (Sequant column; 2.1 × 150 mm) was used for separation. Cycle time was 100 ms. Collision energies and product ions (MS2 or quantifier and qualifier ion transitions) were optimized. Electrospray ionization source conditions were set as follows: gas temperature, 250 °C; gas flow, 12 liters/min; Nebulizer, 20 psi; sheath gas temperature, 350 °C; cap voltage, 2000 V; and nozzle voltage, 1000 V. The gradient consisted of buffer A and buffer B. Buffer A was 95:5 H_2O:acetonitrile, 20 mM NH_4OAc, 20 mM NH_4OH (pH 9.4). Buffer B was acetonitrile. The gradient with A/B ratios were as follows: T0, 10:90; T1.5, 10:90; T20, 60:40; T25, off. Five microliters was injected. For analysis of lysine metabolites, identical column and chromatography conditions as in the "untargeted metabolomics" section were used. In all cases, a standard curve was recorded and integrated using the mass hunter platform (Agilent). The method for the TCA cycle including transitions was previously published [22]. The transitions used for malonyl-Lysine were as follows: 233 -> 84; 233 -> 129.09, 233 -> 147.10 (for non-labeled malonyl-Lysine) and 239 -> 89, 239 -> 134, 239 -> 153 for 13C6 labeled malonyl-Lysine).

Immunoblot.

Protein samples in RIPA buffer were loaded onto Novex 4–12% Bis-Tris gels (Life Tech) and were transferred onto nitrocellulose membranes with the Novex semi-dry transfer apparatus (Life Tech). After blocking in 5% milk-TBST for 1 h at room temperature, blots were incubated overnight in 5% BSA-TBST (1:1000 acetylated-lysine CST, 1:1000 malonyl-lysine CST, 1:5000 beta-actin Genscript A00702) at 4 deg Celsius. After washing in TBST, blots were incubated in 1:5000 HRP-conjugated secondary antibodies (mouse anti-rabbit Jackson Immunoresearch 211-032-171, rabbit anti-mouse Jackson Immunoresearch 211-035-109) in 1% milk-TBST. Blots were incubated with ECL Western blotting substrate (Pierce

Scientific 32106) and were processed by autoradiography. The used ladder was Biorad Precision Plus All-blue ladder.

Study approval.

All studies using D/SS rats were conducted at Medical College of Wisconsin and protocols were approved by the MCW Animal Care and Use Committees and were performed in accordance with the standards set forth by the NIH Guide for the Care and Use of Laboratory Animals (National Academies Press, 2011). All mice studies were conducted at the MPI for Heart Lung and Blood Research Bad Nauheim as previously described in accordance to the local authorities[31,60,61].

Statistical analysis.

Two-tailed t-tests were used for comparison unless otherwise indicated. Analysis of metabolomics and proteomics data is described in the respective sections.

Declarations

Data availability.

In house Scripts are available through Github (see isotope selection approaches, for correlation based approach https://github.com/hpbenton/targeted_isotopes), and for mass-difference approach https://github.com/xdomingoal/isoTracker. Metabolomics data will be made available through XCMS online. Proteomics data is available through the PRIDE/proteomExchange repository [62,63], http://www.ebi.ac.uk/pride . Project accession: PXD007749. Reviewer account details: Username: reviewer93072@ebi.ac.uk, Password: 9PpJ1Jz5

Author contribution.

Performed experiments. MMR, OP, DG, AP; MLG, MH, NH, BPK

Contributed new reagents/ tools: MAS, NH, MB, BFC, MK, HPB, MH

Analyzed data: MMR, OP, DG, XD-A, AP, CG, TB, JX; MB, HPB

Interpreted data and discussion: MMR, OP, TB, MB, ES, OAW, GS, AS

Acknowledgement.

We would like to thank Vladislav Levchenko, Lashodya Dissanayake and Denisha Spires for their help with collection of materials and work with animals, John Bukowy (all Medical College of Wisconsin) for help with application of convolutional neural nets for the glomerular damage analyses, and Rikke Nielsen (Aarhus University) for critically reading the manuscript, and Volker Vallon (UCSD) for helpful discussions. The authors acknowledge the help of the CECAD proteomics core, and the technical

assistance of Ruth Herzog. This research was supported by the National Institutes of Health grants R35 HL135749 (to A.S) and NIH CA231991 (to B.F.C), American Heart Association grants 17SDG33660149 (to O.P.), Spanish Ministry of Science and Innovation - State Research Agency (AEI) grant PID2019-106277RA-I00 (to X.D-A) and Department of Veteran Affairs I01 BX004024 (to A.S.). M.M.R. was supported by the DFG (Ri2811-1/2, Ri2811-2), and the work is currently supported the Novo Nordisk Foundation Young Investigator Grant to M.M.R., as well as Aarhus University Forskening Fonden (AUFF).

References

1. Jang, C. *et al.* A branched-chain amino acid metabolite drives vascular fatty acid transport and causes insulin resistance. *Nat. Med.* **22**, 421–426 (2016).
2. Wang, T. J. *et al.* 2-Aminoadipic acid is a biomarker for diabetes risk. *J. Clin. Invest.* **123**, 4309–4317 (2013).
3. Hacker, S. M. *et al.* Global profiling of lysine reactivity and ligandability in the human proteome. *Nat. Chem.* **9**, 1181–1190 (2017).
4. Choudhary, C., Weinert, B. T., Nishida, Y., Verdin, E. & Mann, M. The growing landscape of lysine acetylation links metabolism and cell signalling. *Nat. Rev. Mol. Cell Biol.* **15**, 536–550 (2014).
5. Narita, T., Weinert, B. T. & Choudhary, C. Functions and mechanisms of non-histone protein acetylation. *Nat. Rev. Mol. Cell Biol.* **20**, 156–174 (2019).
6. Hirschey, M. D. & Zhao, Y. Metabolic Regulation by Lysine Malonylation, Succinylation, and Glutarylation. *Mol. Cell. Proteomics MCP* **14**, 2308–2315 (2015).
7. Tan, M. *et al.* Lysine glutarylation is a protein posttranslational modification regulated by SIRT5. *Cell Metab.* **19**, 605–617 (2014).
8. Zhang, D. *et al.* Metabolic regulation of gene expression by histone lactylation. *Nature* **574**, 575–580 (2019).
9. Gaffney, D. O. *et al.* Non-enzymatic Lysine Lactoylation of Glycolytic Enzymes. *Cell Chem. Biol.* **27**, 206-213.e6 (2020).
10. Sibbersen, C. & Johannsen, M. Dicarbonyl derived post-translational modifications: chemistry bridging biology and aging-related disease. *Essays Biochem.* **64**, 97–110 (2020).
11. Rinschen, M. M., Ivanisevic, J., Giera, M. & Siuzdak, G. Identification of bioactive metabolites using activity metabolomics. *Nat. Rev. Mol. Cell Biol.* **20**, 353–367 (2019).
12. Chronic Kidney Disease (CKD) Surveillance Project. https://nccd.cdc.gov/CKD/.
13. Mills, K. T., Stefanescu, A. & He, J. The global epidemiology of hypertension. *Nat. Rev. Nephrol.* **16**, 223–237 (2020).
14. Li, Y. *et al.* Genome-Wide Association Studies of Metabolites in Patients with CKD Identify Multiple Loci and Illuminate Tubular Transport Mechanisms. *J. Am. Soc. Nephrol. JASN* **29**, 1513–1524 (2018).

15. Schlosser, P. *et al.* Genetic studies of urinary metabolites illuminate mechanisms of detoxification and excretion in humans. *Nat. Genet.* **52**, 167–176 (2020).
16. Köttgen, A. *et al.* New loci associated with kidney function and chronic kidney disease. *Nat. Genet.* **42**, 376–384 (2010).
17. McMahon, G. M. *et al.* Urinary metabolites along with common and rare genetic variations are associated with incident chronic kidney disease. *Kidney Int.* **91**, 1426–1435 (2017).
18. Cheng, Y. *et al.* Urinary Metabolites Associated with Blood Pressure on a Low- or High-Sodium Diet. *Theranostics* **8**, 1468–1480 (2018).
19. Rebholz, C. M., Lichtenstein, A. H., Zheng, Z., Appel, L. J. & Coresh, J. Serum untargeted metabolomic profile of the Dietary Approaches to Stop Hypertension (DASH) dietary pattern. *Am. J. Clin. Nutr.* **108**, 243–255 (2018).
20. Chen, L. *et al.* Sodium Reduction, Metabolomic Profiling, and Cardiovascular Disease Risk in Untreated Black Hypertensives. *Hypertens. Dallas Tex 1979* **74**, 194–200 (2019).
21. Capellades, J. *et al.* geoRge: A Computational Tool To Detect the Presence of Stable Isotope Labeling in LC/MS-Based Untargeted Metabolomics. *Anal. Chem.* **88**, 621–628 (2016).
22. Rinschen, M. M. *et al.* Metabolic rewiring of the hypertensive kidney. *Sci. Signal.* **12**, (2019).
23. Bukowy, J. D. *et al.* Region-Based Convolutional Neural Nets for Localization of Glomeruli in Trichrome-Stained Whole Kidney Sections. *J. Am. Soc. Nephrol. JASN* **29**, 2081–2088 (2018).
24. Clark, J. Z. *et al.* Representation and relative abundance of cell-type selective markers in whole-kidney RNA-Seq data. *Kidney Int.* **95**, 787–796 (2019).
25. Thelle, K., Christensen, E. I., Vorum, H., Ørskov, H. & Birn, H. Characterization of proteinuria and tubular protein uptake in a new model of oral L-lysine administration in rats. *Kidney Int.* **69**, 1333–1340 (2006).
26. Eshbach, M. L. & Weisz, O. A. Receptor-Mediated Endocytosis in the Proximal Tubule. *Annu. Rev. Physiol.* **79**, 425–448 (2017).
27. Shimomura, A. *et al.* Dietary l-Lysine Prevents Arterial Calcification in Adenine-Induced Uremic Rats. *J. Am. Soc. Nephrol.* **25**, 1954–1965 (2014).
28. Puchalska, P. *et al.* Isotope Tracing Untargeted Metabolomics Reveals Macrophage Polarization-State-Specific Metabolic Coordination across Intracellular Compartments. *iScience* **9**, 298–313 (2018).
29. Dethloff, F., Bueschl, C., Heumann, H., Schuhmacher, R. & Turck, C. W. Partially 13C-labeled mouse tissue as reference for LC-MS based untargeted metabolomics. *Anal. Biochem.* **556**, 63–69 (2018).
30. Hölper, S., Ruhs, A. & Krüger, M. Stable isotope labeling for proteomic analysis of tissues in mouse. *Methods Mol. Biol. Clifton NJ* **1188**, 95–106 (2014).
31. Krüger, M. *et al.* SILAC mouse for quantitative proteomics uncovers kindlin-3 as an essential factor for red blood cell function. *Cell* **134**, 353–364 (2008).

32. Nolte, H., Hölper, S., Selbach, M., Braun, T. & Krüger, M. Assessment of serum protein dynamics by native SILAC flooding (SILflood). *Anal. Chem.* **86**, 11033–11037 (2014).
33. Kang, H. M. *et al.* Defective fatty acid oxidation in renal tubular epithelial cells has a key role in kidney fibrosis development. *Nat. Med.* **21**, 37–46 (2015).
34. Katsyuba, E. *et al.* De novo NAD+ synthesis enhances mitochondrial function and improves health. *Nature* **563**, 354–359 (2018).
35. Ralto, K. M., Rhee, E. P. & Parikh, S. M. NAD+ homeostasis in renal health and disease. *Nat. Rev. Nephrol.* **16**, 99–111 (2020).
36. Tran, M. T. *et al.* PGC1α drives NAD biosynthesis linking oxidative metabolism to renal protection. *Nature* **531**, 528–532 (2016).
37. Kirabo, A. *et al.* DC isoketal-modified proteins activate T cells and promote hypertension. *J. Clin. Invest.* **124**, 4642–4656 (2014).
38. Wang, X., Desai, K., Clausen, J. E. S. T. & Wu, L. Increased methylglyoxal and advanced glycation end products in kidney from spontaneously hypertensive rats. *Kidney Int.* **66**, 2315–2321 (2004).
39. Perkovic, V. *et al.* Canagliflozin and Renal Outcomes in Type 2 Diabetes and Nephropathy. *N. Engl. J. Med.* **380**, 2295–2306 (2019).
40. Packer, M. *et al.* Cardiovascular and Renal Outcomes with Empagliflozin in Heart Failure. *N. Engl. J. Med.* **0**, null (2020).
41. Torres, J. A. *et al.* Ketosis Ameliorates Renal Cyst Growth in Polycystic Kidney Disease. *Cell Metab.* **30**, 1007-1023.e5 (2019).
42. Tautenhahn, R., Patti, G. J., Rinehart, D. & Siuzdak, G. XCMS Online: a web-based platform to process untargeted metabolomic data. *Anal. Chem.* **84**, 5035–5039 (2012).
43. Höhne, M. *et al.* Single-nephron proteomes connect morphology and function in proteinuric kidney disease. *Kidney Int.* **93**, 1308–1319 (2018).
44. Cox, J. & Mann, M. MaxQuant enables high peptide identification rates, individualized p.p.b.-range mass accuracies and proteome-wide protein quantification. *Nat. Biotechnol.* **26**, 1367–1372 (2008).
45. Rinschen, M. M. *et al.* A Multi-layered Quantitative In Vivo Expression Atlas of the Podocyte Unravels Kidney Disease Candidate Genes. *Cell Rep.* **23**, 2495–2508 (2018).
46. Tyanova, S. *et al.* The Perseus computational platform for comprehensive analysis of (prote)omics data. *Nat. Methods* **13**, 731–740 (2016).
47. Cowley, A. W. *et al.* Progression of glomerular filtration rate reduction determined in conscious Dahl salt-sensitive hypertensive rats. *Hypertens. Dallas Tex 1979* **62**, 85–90 (2013).
48. Palygin, O. *et al.* Essential role of Kir5.1 channels in renal salt handling and blood pressure control. *JCI Insight* **2**, (2017).
49. Pavlov, T. S. *et al.* Deficiency of renal cortical EGF increases ENaC activity and contributes to salt-sensitive hypertension. *J. Am. Soc. Nephrol. JASN* **24**, 1053–1062 (2013).

50. Endres, B. T. *et al.* Mutation of Plekha7 attenuates salt-sensitive hypertension in the rat. *Proc. Natl. Acad. Sci. U. S. A.* **111**, 12817–12822 (2014).
51. Ren, Q. *et al.* Shear stress and oxygen availability drive differential changes in opossum kidney proximal tubule cell metabolism and endocytosis. *Traffic Cph. Den.* **20**, 448–459 (2019).
52. Long, K. R. *et al.* Proximal tubule apical endocytosis is modulated by fluid shear stress via an mTOR-dependent pathway. *Mol. Biol. Cell* **28**, 2508–2517 (2017).
53. Sandoval, R. M., Molitoris, B. A. & Palygin, O. Fluorescent Imaging and Microscopy for Dynamic Processes in Rats. *Methods Mol. Biol. Clifton NJ* **2018**, 151–175 (2019).
54. Endres, B. T. *et al.* Intravital imaging of the kidney in a rat model of salt-sensitive hypertension. *Am. J. Physiol. Renal Physiol.* **313**, F163–F173 (2017).
55. Zaika, O. L. *et al.* Direct inhibition of basolateral Kir4.1/5.1 and Kir4.1 channels in the cortical collecting duct by dopamine. *Am. J. Physiol. Renal Physiol.* **305**, F1277-1287 (2013).
56. Ilatovskaya, D. V. *et al.* A NOX4/TRPC6 Pathway in Podocyte Calcium Regulation and Renal Damage in Diabetic Kidney Disease. *J. Am. Soc. Nephrol. JASN* **29**, 1917–1927 (2018).
57. Palygin, O. *et al.* Progression of diabetic kidney disease in T2DN rats. *Am. J. Physiol. Renal Physiol.* **317**, F1450–F1461 (2019).
58. Raij, L., Azar, S. & Keane, W. Mesangial immune injury, hypertension, and progressive glomerular damage in Dahl rats. *Kidney Int.* **26**, 137–143 (1984).
59. Kuhl, C., Tautenhahn, R., Böttcher, C., Larson, T. R. & Neumann, S. CAMERA: An integrated strategy for compound spectra extraction and annotation of LC/MS data sets. *Anal. Chem.* **84**, 283–289 (2012).
60. Zanivan, S., Krueger, M. & Mann, M. In vivo quantitative proteomics: the SILAC mouse. *Methods Mol. Biol. Clifton NJ* **757**, 435–450 (2012).
61. Hölper, S., Nolte, H., Bober, E., Braun, T. & Krüger, M. Dissection of metabolic pathways in the Db/Db mouse model by integrative proteome and acetylome analysis. *Mol. Biosyst.* **11**, 908–922 (2015).
62. Perez-Riverol, Y. *et al.* The PRIDE database and related tools and resources in 2019: improving support for quantification data. *Nucleic Acids Res.* **47**, D442–D450 (2019).
63. Vizcaíno, J. A. *et al.* ProteomeXchange provides globally coordinated proteomics data submission and dissemination. *Nat. Biotechnol.* **32**, 223–226 (2014).

Figures

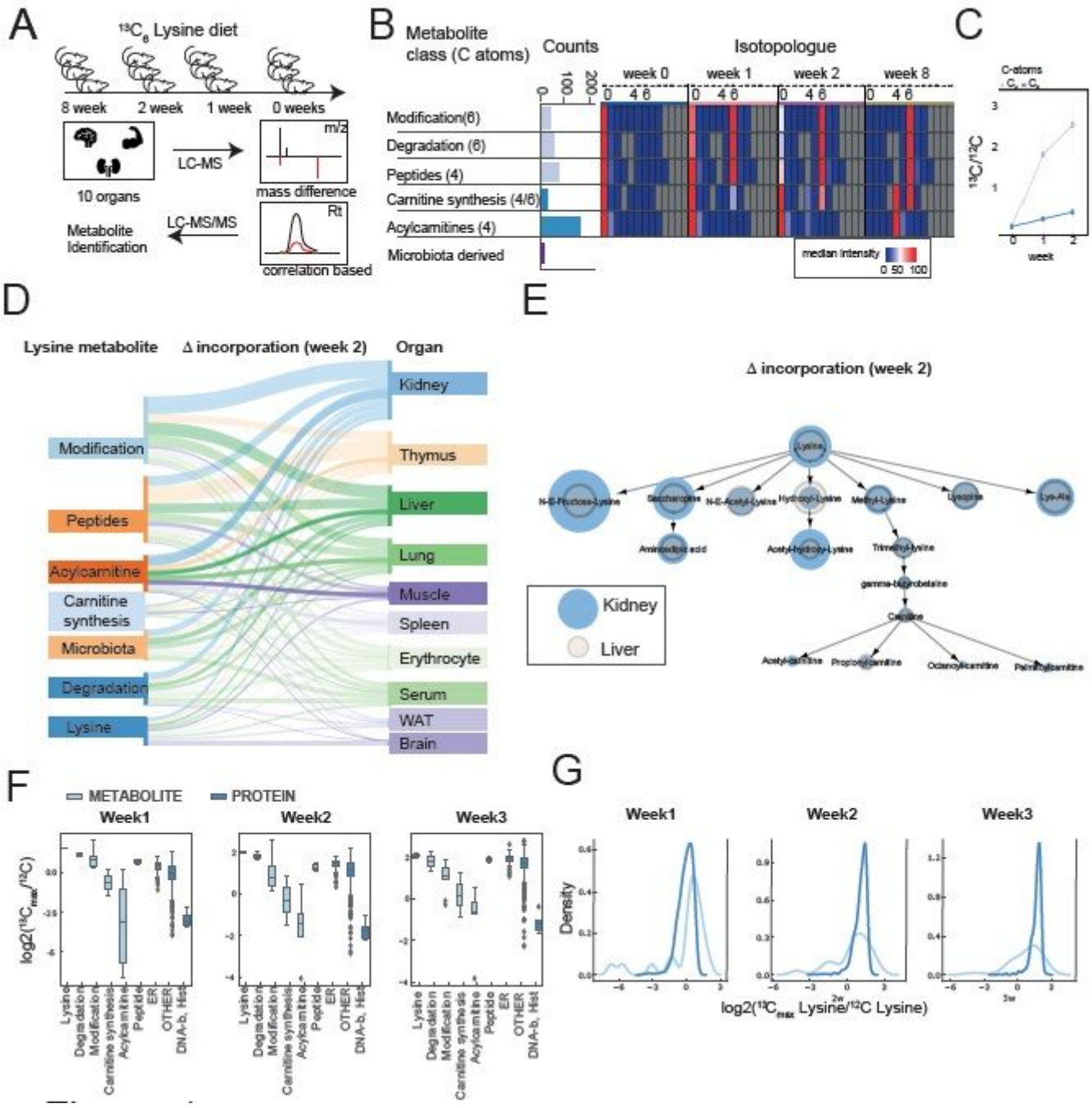

Figure 1

Untargeted analysis of the lysine-labeled metabolome reveals organ-specific lysine handling. A. Mice were labeled in triplicates with food containing exclusively 13C6 Lysine for 1, 2 and 8 weeks. B. Overview of main labeled metabolite classes, and their combined isotopologue patterns over time. C. Slope of isotope incorporation of lysine metabolites with C4 vs C6 backbone. D. Sankey diagram summarizing incorporation slopes of different classes of lysine metabolites in different organs. E. Comparison of slopes of incorporations in liver vs kidney. F. Comparison of lysine incorporation into the metabolome and the proteome of kidney cortex. G. Density of lysine incorporation into the metabolome and proteome of the kidney cortex.

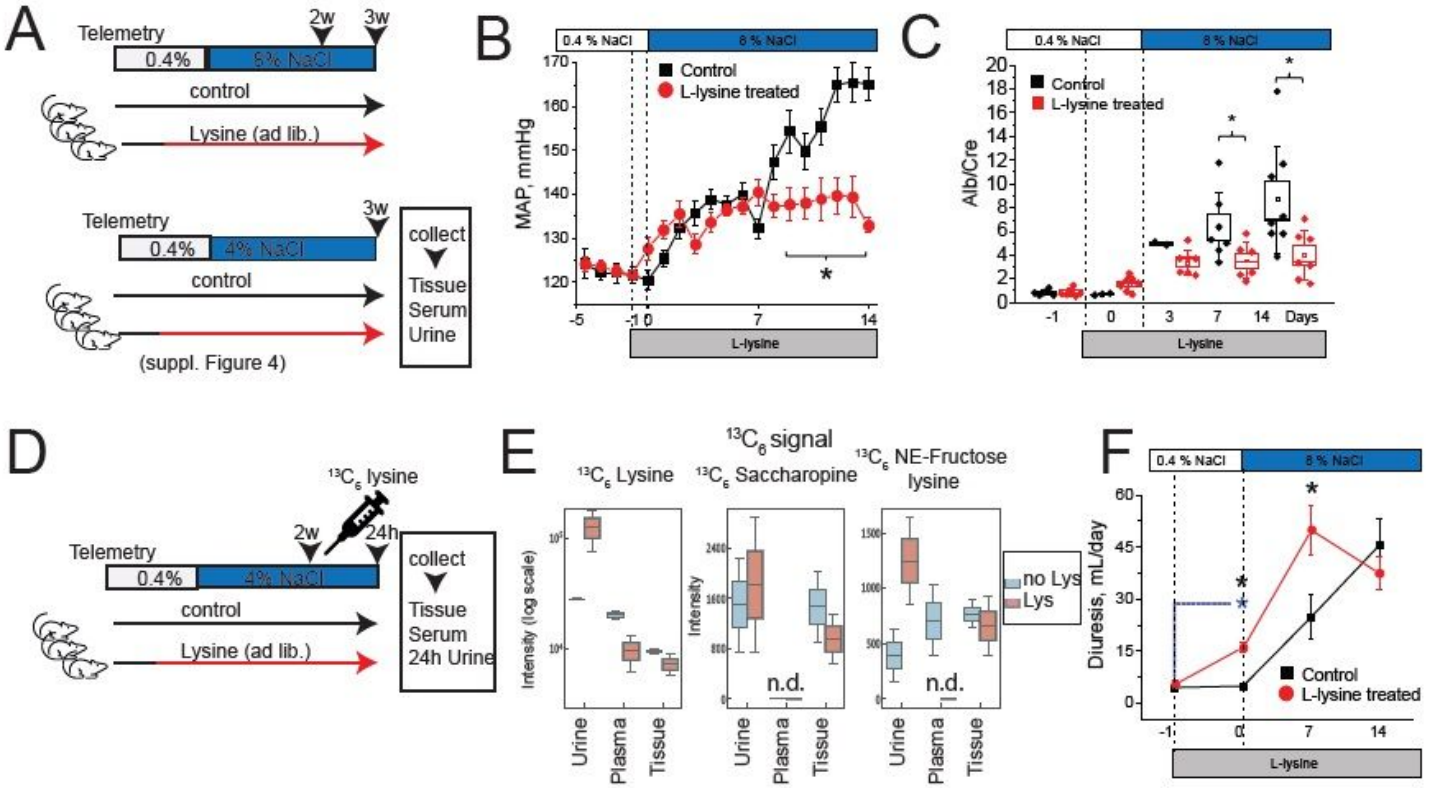

Figure 2

Counteracting lysine deficiency in hypertension ameliorates the disease by physiological mechanisms. A. Lysine administration protocol for rats. B. Mean arterial pressure (MAP) in male D/SS rats under L-lysine treatment. C. Albuminuria (normalized to creatinine) in control and L-lysine treated D/SS rats. D. 13C6 lysine administration and lysine treatment protocol for rats. 13C isotope labeled lysine treatment protocol to analyze lysine trace in presence of excess lysine. E. Metabolomic analysis and signal distribution of 13C6 lysine metabolites in urine, plasma, and kidney tissue. F. Lysine amplifies hypertension-induced diuresis (diuresis/24h).

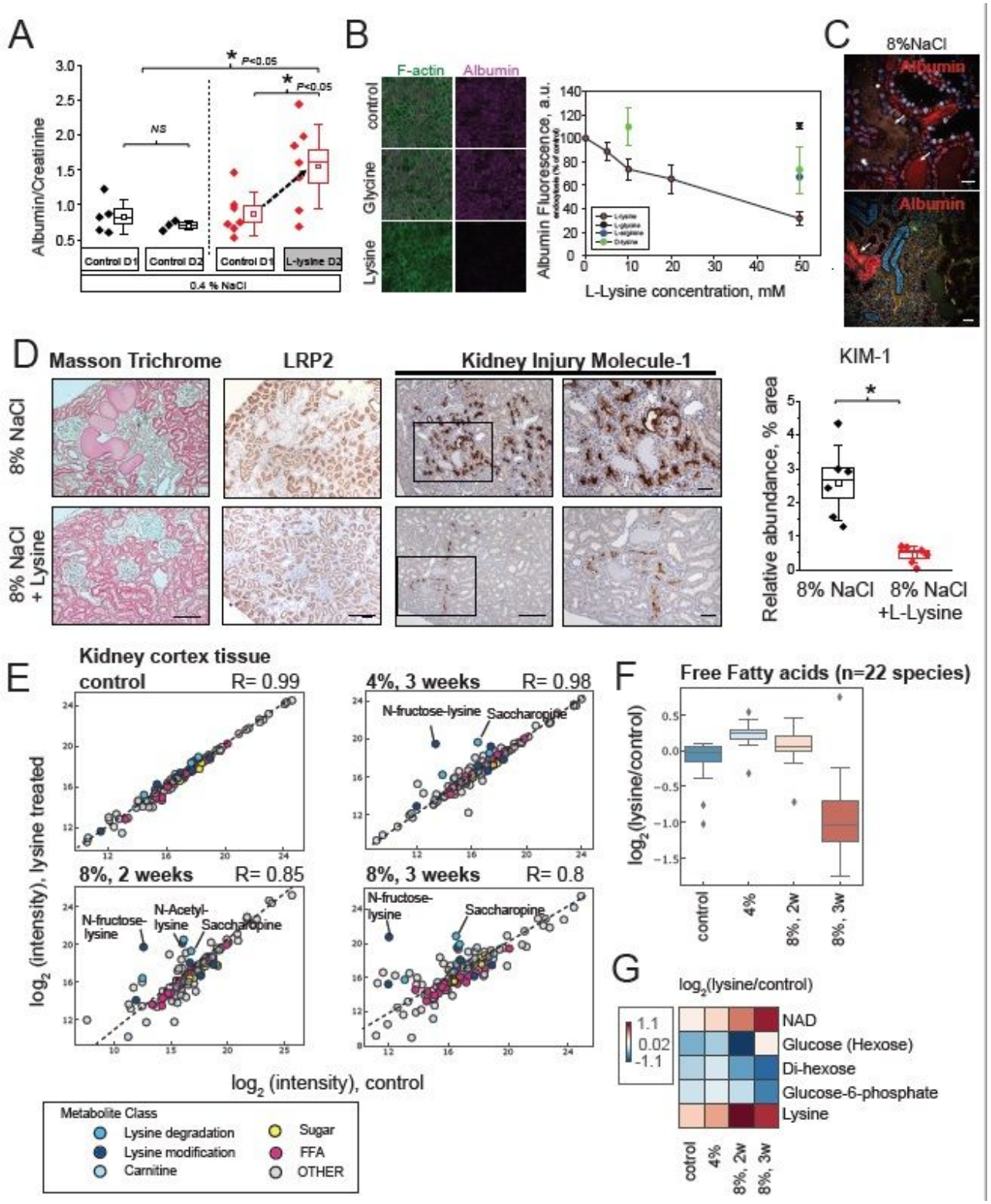

Figure 3

Lysine treatment targets the proximal tubule. A. Urinary Albumin/Creatinine ratio of lysine treated D/SS rats on a normal salt diet. B. Lysine blocks albumin uptake in the proximal tubule cells (OK cell culture) (right panel; green F-actin, magenta fluorescent-labeled albumin). Dose-response showed the inhibition of proximal tubule cell albumin uptake by different lysine concentrations. C. In vivo dual-photon imaging of protein casts and albumin endocytosis by dual photon microscopy. Microscopy shows albumin

endocytosis (labeled red), and saturated albumin uptake in hypertensive D/SS rats D. Lysine supplement prevents proximal tubule injury in SS rats on a high salt diet. Reduction of tissue damage and protein plugs with lysine. Substantial reduction in megalin abundance (LRP2) in dilated proximal tubules can be restored by lysine supplementation. The presence of KIM-1 on the proximal tubule apical membrane shows severe kidney injury in the hypertensive rat on 14D HS (8% NaCl). In contrast, the group supplemented with lysine had a significant reduction in KIM-1 staining. The scale bar is 100 μm. E. Lysine proximal tubule metabolism is altered when kidneys are damaged. Different metabolite classes are color-coded. Metabolites changed with q=0.05 in at least one experiment are depicted. In total, 89 metabolites were significantly altered. F. Decrease of free fatty acids in hypertensive kidneys of lysine-treated animals. The boxplot shows a summary of the regulation of 22 quantified free fatty acids (both saturated and unsaturated). G: Decrease of sugar metabolites glucose and di-hexose, and increase of NAD in lysine treatment in hypertension.

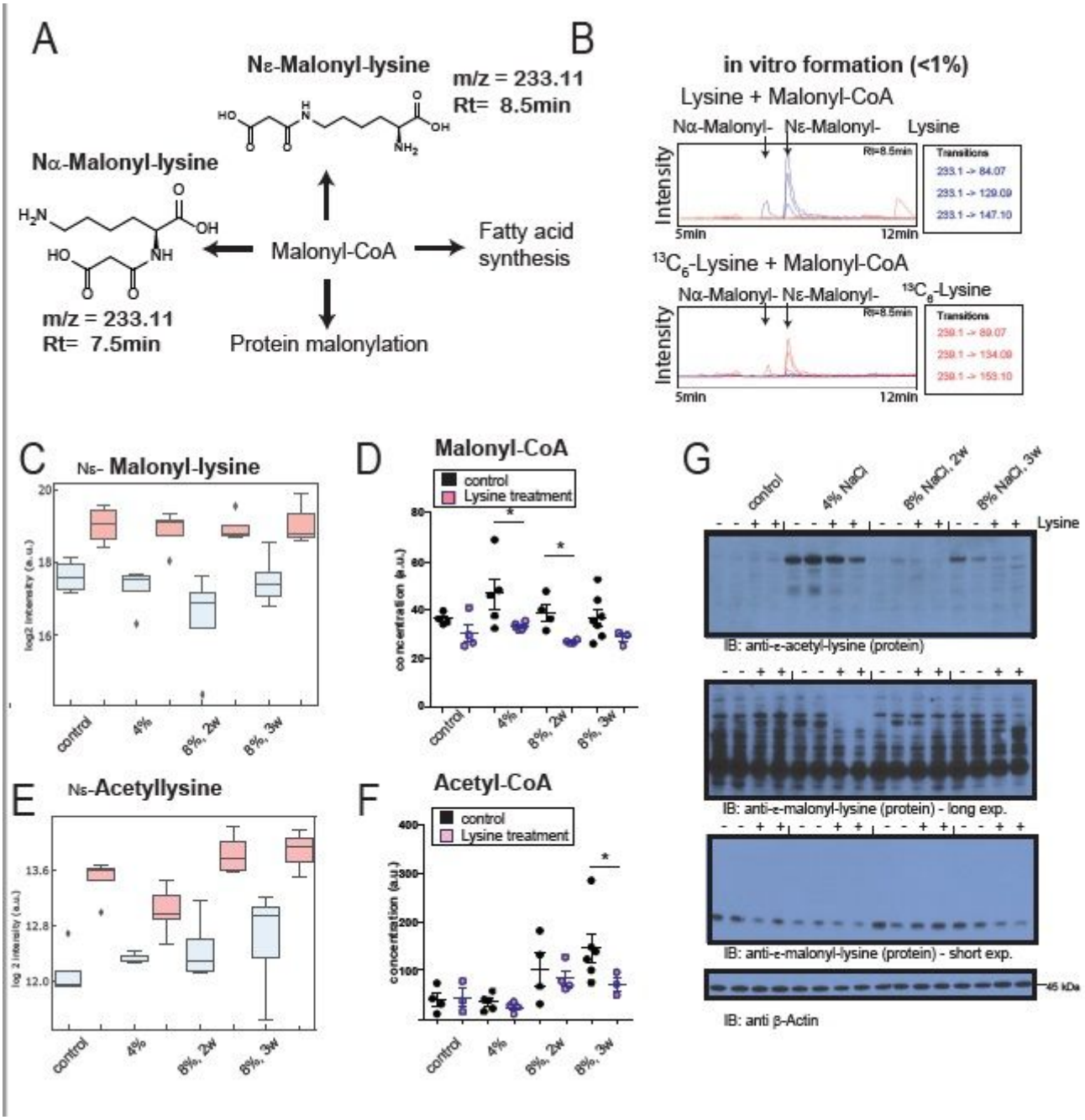

Figure 4

Novel metabolite malonyl-lysine connects lysine metabolism to reduced fatty acid synthesis A. Structure and potential formation of Malonyl-lysine, a previously undescribed metabolite and potentially relationship to fatty acid synthesis. B. Non-enzymatic formation of N-Malonyl-lysine by incubation of lysine and Malonyl-CoA. Both 13C6 and 12C6 lysine were used in the reaction, and detected by targeted metabolomics assay with heavy and light transitions. C. N-Malonyl-lysine abundance in kidney cortices of hypertensive animals with and without lysine treatment (n=4-5, $p<0.05$ in a two-tailed t-test). D. N-Malonyl-lysine abundance in kidney cortices of hypertensive animals with and without lysine treatment. E. N-Acetyl-lysine abundance in kidney cortices. F. Acetyl-CoA abundance in kidney cortices. G. Immunoblot analysis of proteinacetylation and malonylation in cortex lysates as detected with respective antibodies. β-Actin serves as loading control.

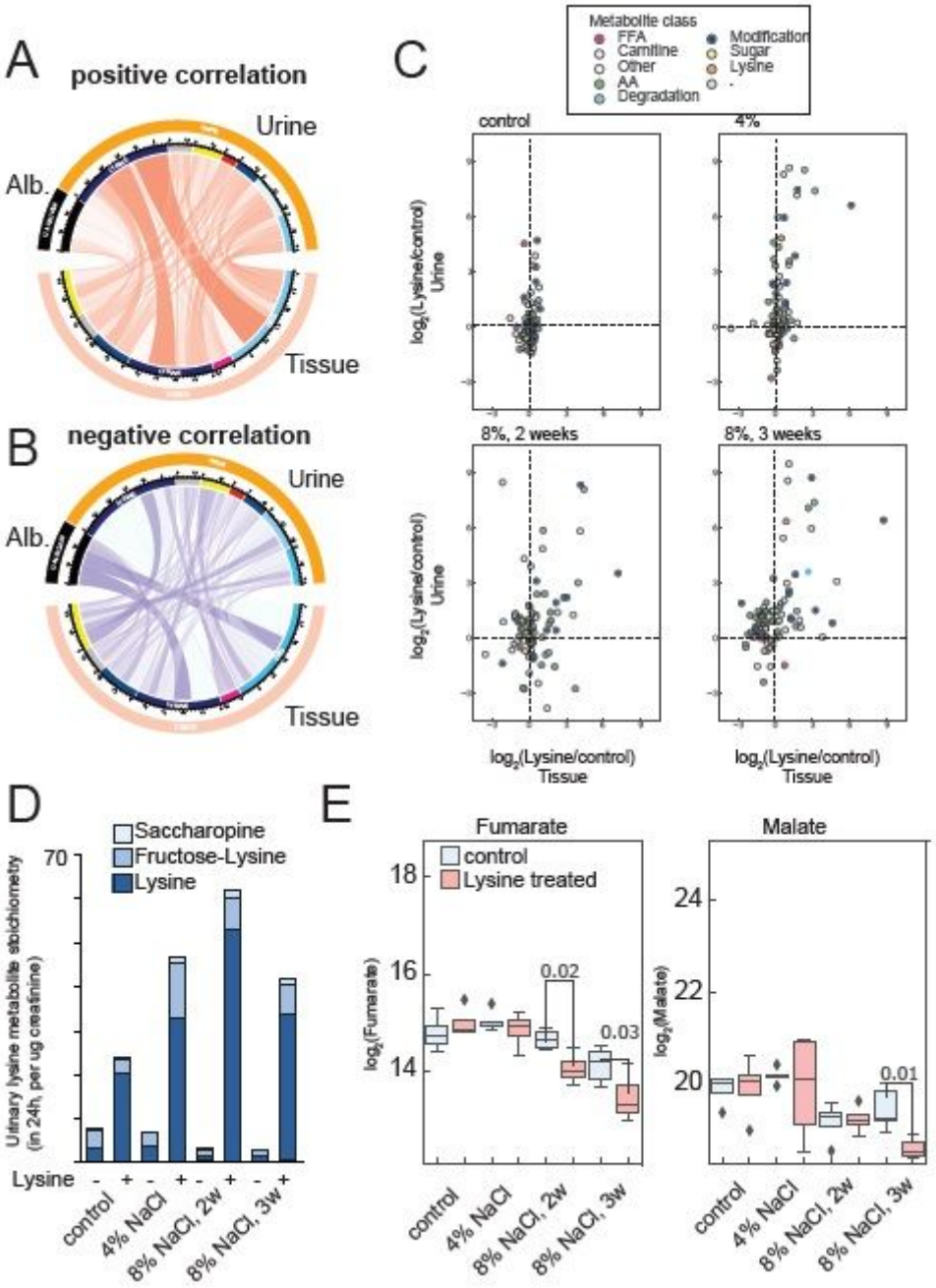

Figure 5

Urine is a sink for lysine conjugate metabolites. A. Integrative analysis depicting kidney and urine metabolite correlation. Chord diagram depicting positive correlations between kidney tissue metabolites and the respective urinary classes. B. Chord diagram depicting negative correlations between kidney tissue metabolites and the respective urinary classes. Strongest negative correlations were 1) Albumin and Lysine in the cortex; 2) Albumin and lysine degradation products in the cortex, and 3) lysine and sugar metabolites in the cortex. C. Scatterplot depicting log2 fold-changes (lysine vs control) in urinary metabolites and kidney cortex metabolites in untargeted metabolomics analysis. The different metabolite classes are color coded. D: Urinary lysine metabolite stoichiometry as determined by targeted metabolomics analysis in 24h collected urine normalized by urinary creatinine. E. Depletion of terminal TCA cycle metabolites by lysine treatment as determined by targeted metabolomics analysis (n=5 per group, two-tailed t-test).

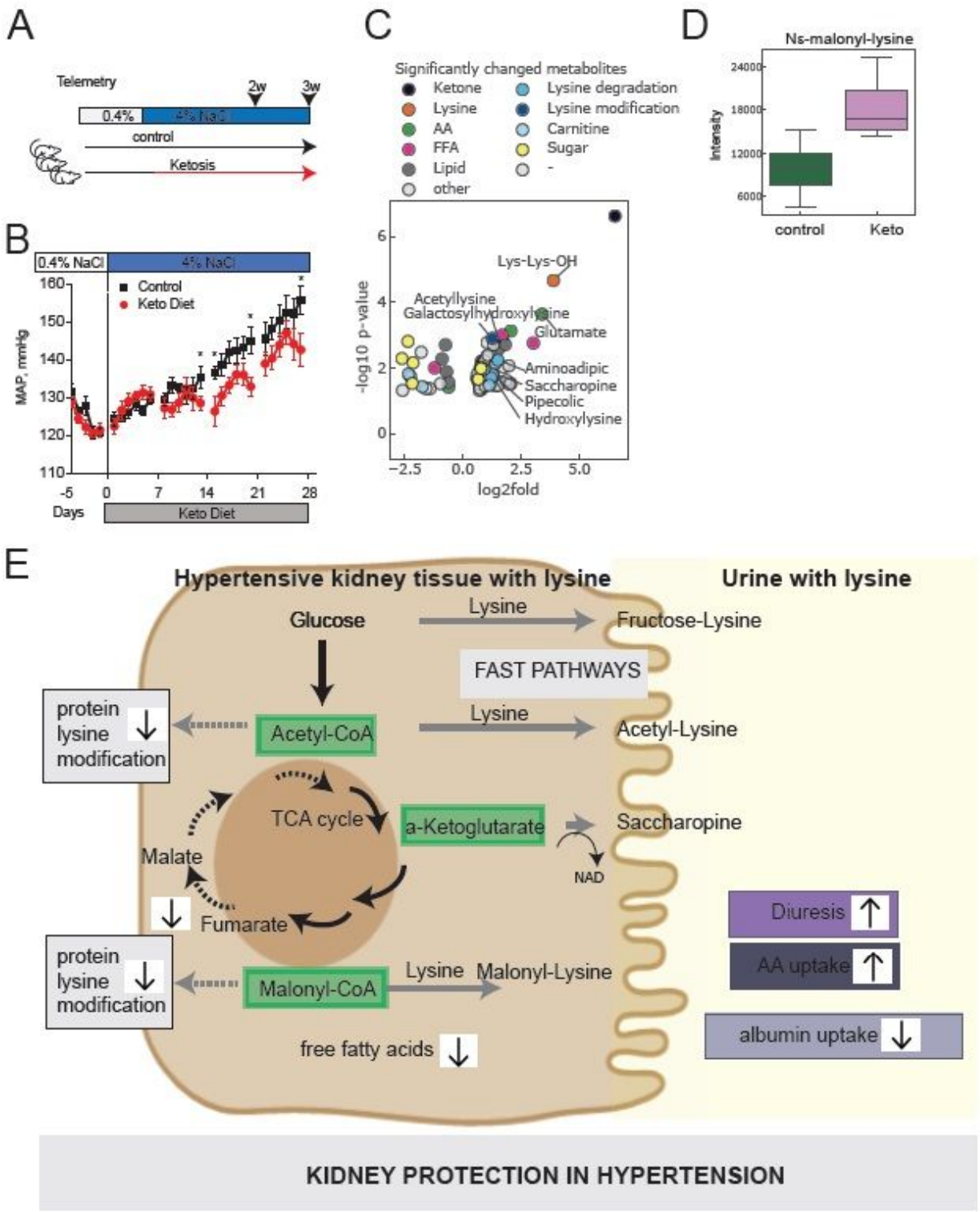

Figure 6

Ketogenic diet, an antihypertensive regime, disturbs modified lysine balance. A. Ketosis protocol. B. Effect of ketogenic diet on the mean arterial pressure (MAP). * indicate significantly changed blood pressure. C. Untargeted metabolomics study of kidney cortex in ketosis and determination of significantly changed metabolites by volcano plot analysis.. D. N-malonyl-lysine in kidney cortex as determined by semi-targeted metabolomics analysis. E. Summary finding depicting lysine-dependent kidney protection by

metabolome alterations by shifting cellular metabolism and sinking central carbon metabolites in the urine.

Supplementary Files

This is a list of supplementary files associated with this preprint. Click to download.

- 201030SupplementalFigure.pdf
- SupplementalMaterial.docx